Journal of Catalysis 276 (2010) 92–100

Contents lists available at ScienceDirect

Journal of Catalysis

journal homepage: www.elsevier.com/locate/jcat

Descriptors controlling the catalytic activity of metallic surfaces toward water splitting

José L.C. Fajín [a], M. Natália D.S. Cordeiro [a], Francesc Illas [b,*], José R.B. Gomes [c,*]

[a] REQUIMTE, Faculdade de Ciências, Universidade do Porto, P-4169-007 Porto, Portugal
[b] IQTCUB, Department de Química Física & Institut de Química Teòrica i Computacional, and ICREA, Institució Catalana de Recerca i Estudis Avançats, University of Barcelona, C/Martí i Franquès 1, 08028 Barcelona, Spain
[c] CICECO, Departamento de Química, Universidade de Aveiro, 3810-193 Aveiro, Portugal

ARTICLE INFO

Article history:
Received 11 May 2010
Revised 30 August 2010
Accepted 4 September 2010
Available online 13 October 2010

Keywords:
Density functional theory
Water gas shift reaction
Periodic slab approach
Brønsted–Evans–Polanyi relationship
Catalytic activity
Surfaces

ABSTRACT

Periodic density functional theory (DFT) calculations have been used to unravel the existence of Brønsted–Evans–Polanyi (BEP) relationships for water dissociation on metallic surfaces which constitutes the rate determining step for the technologically important water gas shift reaction. In addition, it is predicted that nickel surfaces possessing low coordinated atoms could be effective for catalyzing water dissociation. Finally, it is shown that the adsorption energy of atomic oxygen on a given metallic surface provides an excellent descriptor of the activation energy for water dissociation on that surface, thus allowing the screening of large number of metallic and bimetallic systems in a simple way.

1. Introduction

The water gas shift reaction (WGS) ($CO + H_2O \rightarrow CO_2 + H_2$) is a very important chemical process which is used in industry for methanol synthesis, methanol steam reforming and to clean the hydrogen used in the fuel cells [1–3]. The hydrogen-rich gas stream, usually produced from reforming of crude oil, coal, natural gas, wood or biomass, contains ~10% of CO which may degrade the performance of the catalysts used in the subsequent industrial processes. In particular, CO strongly poisons the Pt electrode used in the fuel cell systems [4], and, therefore, the WGS is used to remove the CO gas from the hydrogen-rich gas stream. In industry, the WGS is usually performed with the aid of Cu-based catalysts in the form of nanoparticles dispersed on a ZnO/Al_2O_3 support [see [5,6] and references therein] although Au is increasingly being investigated [7,8]. The metal surface constitutes the catalyst active phase but other factors such as nature of the support, existence of oxygen vacancies, or catalyst preparation process may significantly affect the catalytic activity and the overall catalyst performance [9–12]. Very recently, inverse catalysts – active oxide nanoparticles dispersed on a noble metal support – were suggested as new promising alternatives [13,14].

The possible reaction mechanisms for the WGS on metal-supported catalysts – associative or redox routes – were investigated recently by density functional theory (DFT), considering the Cu(1 1 1) flat surface as the catalyst model, and including a complete microkinetic analysis [15]. It was found that the reaction was more favorable through the associative mechanism – with carboxyl as an intermediate assisted by co-adsorbed OH – and that water dissociation was the rate-limiting step. Considering stepped surface models did not change the main conclusions reached from the planar surface but revealed that the presence of steps and low coordinated atoms significantly reduce the reaction barriers [16]. Water dissociation was also found to be the rate-limiting step but comparing results of the planar and stepped surfaces it was suggested a Brønsted–Evans–Polanyi (BEP) relationship [17,18] between the reaction barrier and the co-adsorption energy (E_{ads}) of the products ($H^* + OH^*$). BEP curves for the WGS have been reported for the (1 1 1) surface of several transition metals [19–21]. Useful BEP relationships have also been proposed for C–C and C–O bonds cleavage reaction during methanol decomposition, and for hydrogenation and dehydrogenation of ethylene on different Pd overlayer surfaces, among others [22–25].

Unfortunately, the relationships discussed above for the WGS do not account for the important role of low coordinated atoms [16]. In fact, the inclusion of stepped surfaces in the derivation of BEP relationships is a necessary requirement, especially after the recent work or Hendriksen et al. emphasizing the importance of

* Corresponding authors. Fax: +34 93 402 1231 (F. Illas), +351 234 370 004 (J.R.B. Gomes).
E-mail addresses: francesc.illas@ub.edu (F. Illas), jrgomes@ua.pt (J.R.B. Gomes).

0021-9517/$ - see front matter © 2010 Elsevier Inc. All rights reserved.
doi:10.1016/j.jcat.2010.09.007

steps and of steps density in catalytic reactions [26]. A general BEP relationship for the water splitting reaction including a larger number of metals and different metallic surfaces of increasing complexity is appealing and urgently needed since it would provide new important information concerning the chemical factors governing water splitting at metal surfaces and, while not directly allowing the design of new and improved catalysts for the WGS and related processes, will no doubt help to contribute to such important goal. Herewith, we go one step beyond relationships and report DFT-derived correlations between the activation energy for water dissociation (E_{act}) on several transition metal (TM) surfaces with different atomic packing – Ni(1 1 1), Pt(1 1 1), Pd(1 1 1), Ir(1 1 1), Cu(1 1 1), Au(1 1 1), Cu(1 1 0), Ni(1 1 0), Ag(1 1 0), Ni(2 1 1), Rh(2 1 1), Cu(3 2 1) and Au(3 2 1) – and the dissociation reaction energy (E_{react}) as expected in a standard BEP relationship but also between E_{act} and the adsorption energy (E_{ads}) of selected adsorbed species ($OH^* + H^*$ or O^*) thus providing useful simple descriptors for this important heterogeneous catalyzed reaction.

2. Catalyst surfaces models and computational details

2.1. Slab models

A series of transition metal (TM) surfaces (Au(1 1 1), Ni(1 1 1), Cu(1 1 1), Pt(1 1 1), Pd(1 1 1), Ag(1 1 0), Ir(1 1 1), Cu(1 1 0), Cu(3 2 1), Au(3 2 1), Ni(1 1 0), Ni(2 1 1) and Rh(2 1 1)) has been chosen to provide a representative group of transition metal surfaces usually employed as catalysts and also to ascertain the role of low coordinated metallic atoms in the dissociation of the first O–H bond of water. In the case of Cu(1 1 1), this has been shown to be the crucial step in the water gas shift reaction (WGS) and we are assuming here that this will also be the case for the rest of transition metals surfaces. In any case, the results from the present study will provide useful data for water dissociation and it is likely that this may be also useful in the context of the WGS reaction. The TM surfaces above were used to compute the energies and structural parameters of adsorbed H_2O, HO + H and O species and to obtain the energy barriers for the $H_2O^* + {}^* \rightarrow OH^* + H^*$ reaction. The data were used to build useful relationships between the activation energy for the reaction of water dissociation and the adsorption energies of selected species or the energy of the dissociation reaction. Finally, note that the set of surfaces used in the present work has not been chosen following the stability order but, as pointed out above, to explore different metals and different surface topologies.

The atomic positions in the slabs used to model the surfaces considered in this work were obtained by cutting the correspondent bulk metals along the desired Miller indices with the CRYSTAL98 computer code [27]. The lattice constants of the metals in their most stable bulk configurations were optimized a priori by spin-polarized-DFT minimization of the energy with respect to the lattice parameter using the VASP 4.6.3 computer code [28–30]. The calculations considered the PW91 generalized gradient approach (GGA) exchange-correlation potential [31], the projected augmented-wave (PAW) method as implemented in VASP [32,33] to take into account the effect of core electrons in the valence electron density, a cutoff of 415 eV for the plane waves expansion and a $15 \times 15 \times 15$ Monkhorst–Pack grid of special k-points [34] for the numerical integration in the reciprocal space. The lattice parameters obtained for the bulk Ni, Pd, Ag, Pt, Ir and Rh metal are 3.522 Å, 3.957 Å, 4.155 Å, 3.986 Å, 3.840 Å and 3.844 Å, respectively, thus showing very good agreement with previous results [20,35,36]. The lattice parameters for Cu and Au were taken from previous work [37,38]. The TM(1 1 1) and TM(1 1 0) surface models consist of 2×2 unit cells with four metallic layers and models used for the TM(2 1 1) surfaces were built from 2×1 unit cells also containing four layers thick. The use of larger unit cells, *i.e.* to simulate lower coverage regimes, was found to have minor influence in the reaction of water dissociation [20].

Some additional TM surfaces, c.f. (Rh(2 2 1), Co(0 0 0 1), Co(1 1 1), Pd(1 1 0), Ir(1 1 0) and Ru(0 0 0 1)), were also considered in this work to validate predictions of activation energy barriers and rate constants based on the relationships proposed without making used of these systems. The slabs were generated in a similar fashion to those reported above. The optimized lattice parameters for hcp-Co, fcc-Co and Ru are 2.487 Å, 3.522 Å and 2.697 Å, respectively, which are in good agreement with values reported previously [36,39–41]. The slabs were generated from repeated 2×2 unit cells, four layers thick, in the case of the TM(1 1 1), TM(0 0 0 1) and TM(1 1 0) surfaces and from a 2×1 unit cell, also four layers thick, for the Rh(2 2 1) surface.

2.2. Adsorption and transition state calculations

The interaction of the different reactants, intermediates and products involved in the water dissociation reaction with the surfaces above was modeled through the repeated slab approach. A vacuum region of ~10 Å in the z direction was introduced into the repeated unit cells for replication in three dimensions. The slabs obtained were further modified by allowing full relaxation, using the conjugate-gradient (CG) algorithm, of the ions in the two uppermost layers with which the reactants are allowed to interact.

The calculations of the gaseous species and of the adsorbates interacting with the TM surfaces were done also using the CG algorithm and same cell sizes. The interactions of OH + H with the different metal surfaces were used for definition of the grids of special k-points. A $7 \times 7 \times 1$ Monkhorst–Pack grid of special k-points was found to be enough for obtaining correct convergence, both in energies and in geometries, for all cases with the exception of the Co(0 0 0 1) surface where it was necessary to use a $9 \times 9 \times 1$ grid. Furthermore, the inclusion of spin polarization into the calculations dealing with the Ni, Pd, Ag, Pt, Ir, Rh, Co and Ru surfaces was found to be crucial.

The PW91 functional was chosen according to a previous work where the performances of different exchange-correlation density functionals were tested for the reaction of water dissociation on the Cu(1 1 1) surface [37]. Herewith, we have considered the PW91 and PBE density functionals to study the first O–H dissociation in water on two additional transition metal surfaces, namely, Ni(1 1 0) and Ag(1 1 0), which originated practically the same results.

The Dimer approach [42] was used to locate the transition state (TS) structures for the $H_2O^* + {}^* \rightarrow OH^* + H^*$ reaction. Tight convergence criteria were 10^{-6} eV for the total energy change and 10^{-3} eV/Å for the forces acting on the ions. These quite strict criteria are necessary in TS searches on the stepped surfaces. Computation of a single imaginary frequency for the configurations obtained with the Dimer method ensured that those were true TS structures.

The harmonic oscillator approach was used to obtain the *zero point vibrational energy* (ZPVE) corrections of the adsorption energy, of the co-adsorption energy, of the reaction energy and of the activation energy barrier. Uncorrected values were also calculated for comparison purposes (with data from previous works without ZPVE-corrections).

Rate constants (k) at 463 K for the water dissociation on the transition metal surfaces mentioned above have been estimated from the transition state theory [43] as in Eq. (1)

$$k = \left(\frac{k_B T}{h}\right)\left(\frac{q^{\neq}}{q}\right) e^{\frac{-E_a}{k_B T}} \quad (1)$$

where k_B is the Boltzmann constant, T is the absolute temperature, h is the Planck constant and E_a the activation energy from the ZPVE corrected calculated energy barrier. Finally, $q^{\neq}$ and q are the partition functions for the TS and initial state, respectively, which have been approximated from the harmonic vibrational frequencies.

3. Results

3.1. Adsorption state of reactants and products

Periodic density functional calculations, using suitable models, have been carried out for the set of surfaces described above and the optimized geometrical parameters of adsorbed water, adsorbed atomic oxygen and also of co-adsorbed hydroxyl and atomic hydrogen at several different sites (hollow, bridge and top positions; see Fig. 1 for adsorption positions) and the corresponding energy have been obtained (complete set of results is given in the Supporting information). Here, let us just point out that for Ni(1 1 1), Ni(1 1 0), Ir(1 1 1), Cu(1 1 1), Pd(1 1 1), Pt(1 1 1) and Au(1 1 1), the calculated PW91 atomic oxygen adsorption energies exhibit a very good correlation ($R^2 = 0.92$) with available experimental data indicating that, for the present purpose, the accuracy of the present computational setup is sufficiently adequate (see Supporting information, Fig. S1).

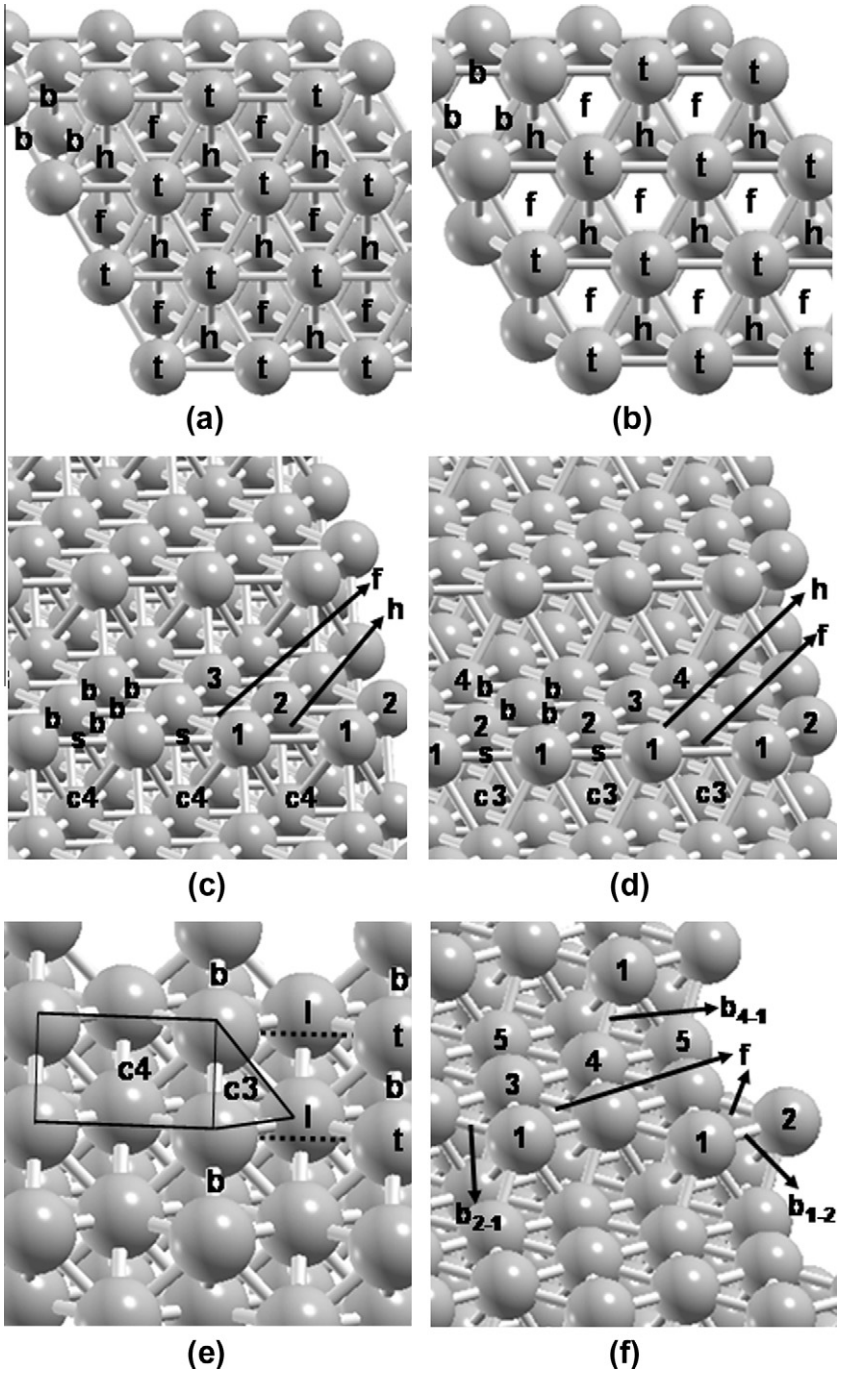

Fig. 1. Adsorption positions at the (a) TM(1 1 1); (b) TM(0 0 0 1); (c) TM(2 1 1); (d) TM(2 2 1); (e) TM(1 1 0) surfaces; and (f) TM(3 2 1) surfaces. Labels are t: top; b: bridge; h: hollow hcp; f: hollow fcc; c3: 3-atoms hollow; c4: 4-atoms hollow; and numbers are used to distinguish different top and bridge sites.

In the case of the TM(1 1 1) surfaces (see Table S1), it is found that the water molecule interacts preferentially with the top sites and with the molecular plane parallel to the surface as found previously [19–21,37]. For H_2O adsorption at these surfaces, E_{ads} values range from −0.18 eV on Au(1 1 1) to −0.32 eV on Ir(1 1 1), and the increasing stability order is Au(1 1 1) < Cu(1 1 1) < Pt(1 1 1) < Pd(1 1 1) < Ni(1 1 1) < Ir(1 1 1). In the case of the folded or stepped surfaces (see also Table S1), the E_{ads} values are larger than those found for the flat (1 1 1) surfaces with energies ranging from −0.34 eV on Au(3 2 1) to −0.61 on Ni(2 1 1), which follows from the preferred interaction of the O atom of the H_2O molecule with the surface atoms with lowest coordination numbers. Finally, it is also interesting to note that, in general, the distance between the oxygen atom and the nearest metal atom in the surface decreases with increasing E_{ads}, reflecting the increasing of the metal–oxygen bond strength. Furthermore, the energetic trends along the periods and groups of the Periodic Table seem to be identical for planar, folded and stepped surfaces as expected from the d-band model [44,45]. Similarly, the (co-)adsorption of the products of water dissociation and of atomic oxygen was investigated for several possible combinations of adsorption sites on the slab models used in the case of water. The calculations were also extended to other surfaces such as Rh(2 2 1), Co(1 1 1), Co(0 0 0 1), Pd(1 1 0), Ir(1 1 0) and Ru(0 0 0 1), since these data are needed to validate subsequent predictions, of E_{act} and rate constants values for water dissociation on these surfaces, based on the BEP relationships obtained from the first set of surfaces (see below). The full set of calculated results, including all vibrational frequencies (Table S5), is given in the Supporting information file (Tables S2 and S3 for co-adsorbed OH + H and for O, respectively).

Water dissociation is found to be thermodynamically unfavorable for all Pt, Pd, Ir, Cu, Ag and Au surfaces considered. It is favorable in the cases of Ni(2 1 1) and Ni(1 1 0) and almost thermoneutral when the dissociation occurs on Rh(2 1 1) and Ni(1 1 1) surfaces. The trend in E_{react} along the Periodic Table follows the prediction of the d-band center model [44,45] whereas co-adsorption is enhanced by the presence of low coordinated atoms [16]. Interestingly, identical E_{react} values are obtained for the two flat cobalt surfaces. These were chosen because the WGS has two working cycles, one at a low temperature where the Co(0 0 0 1) surface is more stable and another at a high temperature where the Co(1 1 1) surface is more stable. Co(1 1 1) and Co(0 0 0 1) surfaces were obtained from cleavage of the *fcc* and *hcp* crystal phases of bulk Co, respectively. In the case of atomic oxygen, the interaction is strongly favorable on the cavities in all the surfaces considered with adsorption energies ranging from −3.01 eV on Au(1 1 1) to −5.70 eV on Co(0 0 0 1), Table S3.

3.2. Activation energy barriers and rate constants

Let us now turn our attention to the E_{act} values which are calculated as the difference between the transition state energy and that of adsorbed water at the most stable configuration. Table 1 reports these data together with the length of the O–H bond at the TS structure and with E_{react} values and transition state theory derived rate constants calculated at a temperature of 463 K (typical value for the low-temperature WGS). Relevant structures along the coordinate of reaction are shown in Fig. 2. From the results in this table, it is clear that the calculated E_{act} for the $H_2O^* + * \rightarrow OH^* + H^*$ reaction on Au(1 1 1) is too high, as expected, being ∼1 eV larger than the values for the other (1 1 1) surfaces. On the other hand, the E_{act} for the other five (1 1 1) surfaces differ by less than 0.3 eV. Au remains the least active catalyst even if low coordinated atoms are available in the surface; see entry for Au(3 2 1) in Table 1. Interestingly, similar E_{act} values are obtained for Ir(1 1 1) and Ni(1 1 1), 0.68 eV and 0.71 eV respectively, but a larger difference is found between barriers calculated for Pt(1 1 1) and Cu(1 1 1), 0.78 eV and 0.91 eV, respectively. Similar to the trend discussed for E_{ads}, the E_{act} values decrease with the presence of low coordinated atoms (compare entries Ni or Cu (1 1 1) with entries Ni or Cu (1 1 0) for surfaces with coordination numbers (CN) of 9 and 7, respectively). Note that the lowering of the energy barrier is not so efficient in the case of the Cu(3 2 1) surface where E_{act} is 0.1 eV larger than the value corresponding to the Cu(1 1 0) surface. This is because in the transition state structure the cleaving hydrogen atom is interacting with the (1 1 1) terraces where CN(Cu) = 9 while in the case of Cu(1 1 0) the two reaction products, OH^* and H^*, are interacting with the outermost surface atoms having CN(Cu) = 7. The calculated reaction energy profile shows that the water dissociation reaction on the surfaces considered is thermodynamically favorable with respect to adsorbed water only in the case of some nickel surfaces. Furthermore, as it can be seen for Ni and Cu, the reaction is more exothermic on (1 1 0) than on (1 1 1) facets. Importantly, the reaction energy on the Ir(1 1 1) sur-

Table 1
DFT calculated parameters for water dissociation on several TM surfaces.

Surface	O···H[a]	E^{O}_{act} [b]	E^{O}_{react} [c]	ΔG[d]	k[e]
Ir(1 1 1)	1.54	0.68	0.43	81.2	1.7×10^5
Ni(1 1 1)	1.55	0.71	−0.37	4.1	7.4×10^4
Pd(1 1 1)	1.70	0.96	0.41	79.5	5.1×10^1
Pt(1 1 1)	1.78	0.78	0.66	103.7	5.1×10^3
Cu(1 1 1)[f,g]	1.47 (1.47)	0.91 (0.92)	0.15 (0.19)	54.5 (57.7)	1.6×10^2 (1.9×10^2)
Au(1 1 1)	2.01	1.88	1.64	198.3	1.5×10^{-9}
Ni(1 1 0)[g]	1.34 (1.34)	0.39 (0.39)	−0.52 (−0.51)	−10.7 (−9.5)	1.8×10^8 (1.9×10^8)
Cu(1 1 0)	1.43	0.61	0.03	43.1	4.0×10^5
Ag(1 1 0)[g]	1.64 (1.65)	1.12 (1.13)	0.85 (0.86)	121.4 (122.7)	2.2×10^1 (2.2×10^1)
Rh(2 1 1)	1.47	0.67	−0.41	0.5	1.2×10^5
Ni(2 1 1)	1.32	0.61	−0.70	−27.8	1.1×10^6
Cu(3 2 1)	1.63	0.71	0.22	61.0	3.6×10^4
Au(3 2 1)	1.86	1.33	1.19	154.6	3.5×10^{-3}
Pd(1 1 0)	1.50	0.73	0.17	64.3	6.9×10^3

[a] HO···H breaking bond in Å.
[b] ZPVE-corrected activation energy barrier in eV.
[c] Reaction energy in eV.
[d] Gibbs free energy (kJ/mol) for the water dissociation at 463 K and 1 bar calculated as in Ref. [20]. Additional details in the supporting information. Note that the information provided by ΔG or E^{O}_{react} is essentially the same.
[e] Reaction rate constant in s^{-1}.
[f] Data from Ref. [37] recalculated using the same computational procedure considered in this work.
[g] Between parenthesis the data calculated with the PBE density functional.

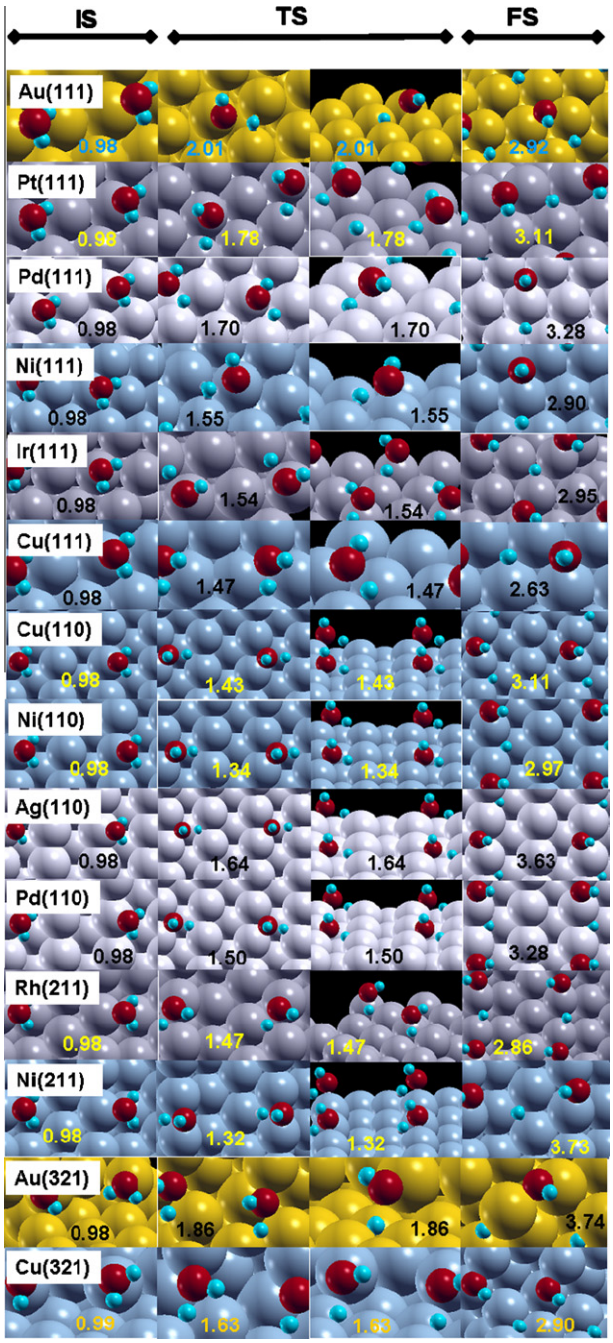

Fig. 2. Optimized structures for the initial (IS), transition (TS) and final (FS) states for the $H_2O^* + * \rightarrow OH^* + H^*$ reaction. Length of the cleaved O–H bond is given in Å.

face, which presents a barrier for water dissociation similar to Ni(1 1 1), is quite endothermic. The calculated rate constants for water dissociation reflect the lower energy barriers found on Ir, Ni, Rh and Cu surfaces and, hence, the rate of the catalytic reaction is expected to be higher than on the other surfaces considered.

3.3. Brønsted–Evans–Polanyi relationships

The data in Table 1 (and also in Tables S1–S4) were used to investigate whether a BEP relationship holds for the WGS. Energies used refer always to the most favorable situations. In fact, the consideration of other options can lead to artifacts in the relationships obtained (c.f. Fig. 2 in Ref. [46]). Hence, we first explore the dependence of E_{act} for the first O–H bond dissociation in adsorbed water with respect to E_{react}. Fig. 3a shows that a BEP relationship does indeed hold which agrees with and generalizes previous findings [19]. Note, however, that the data corresponding to Au surfaces were not considered because of their exceedingly large E_{act} value. The linear trend in Fig. 3a is encouraging since the structures involved in the $H_2O^* + * \rightarrow OH^* + H^*$ reaction differ significantly from surface to surface.

In order to exploit all the possible data, we have also considered a multilinear least square regression between E_{act} versus E_{react}, $E_{ads(OH+H)}$, $E_{ads(O)}$ and $E_{ads(H2O)}$. The outcome of this multilinear fit indicates a good correlation as indicated by Eq. (2) below

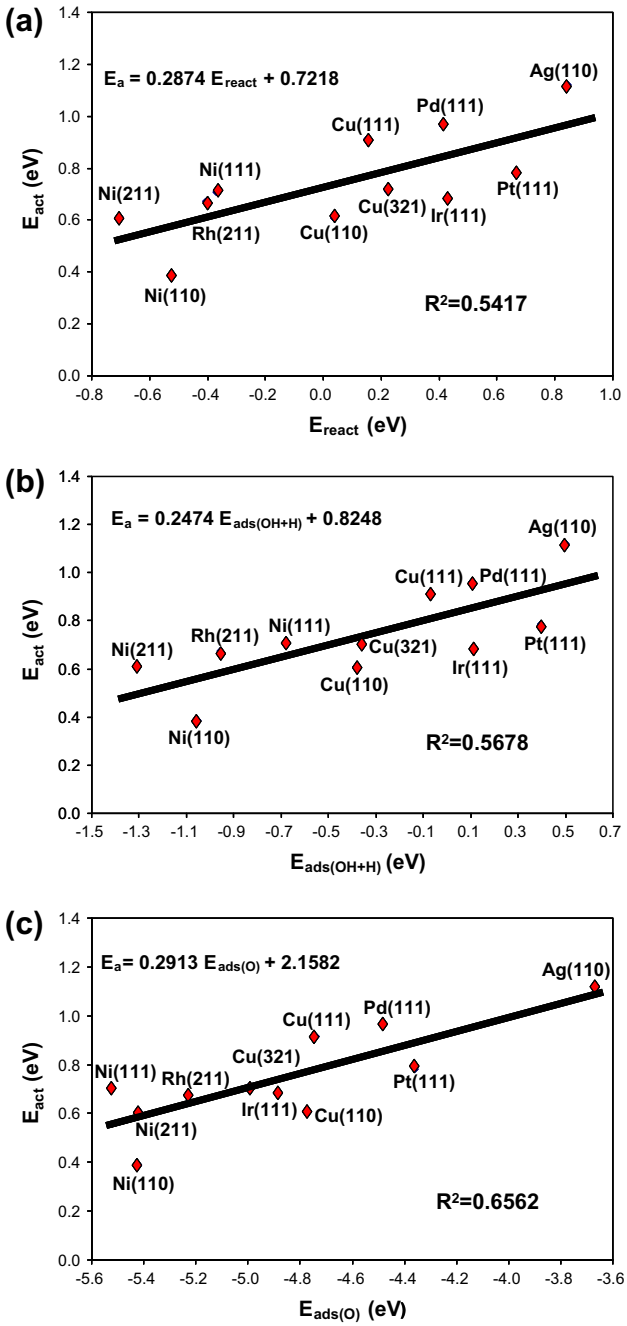

Fig. 3. Relationships between activation energy barriers (E_{act}) and (a) reaction energy (E_{react}), (b) co-adsorption energy of HO and H species, (c) adsorption energy of atomic oxygen. Note that (a) corresponds to the standard BEP relationship while (c) is providing a convenient descriptor for the water splitting reaction.

$$E_{act} = 4.9199E_{react} - 4.9500E_{(OH+H)} + 0.1953E_{ads(O)} + 5.4253E_{ads(H_2O)} + 1.8703 \quad (2)$$

with $R^2 = 0.7281$ and $\Delta = 0.09$ eV although from a pragmatic point of view is less interesting since it requires the calculation of a larger number of quantities.

The BEP relationship in Fig. 3a can be used to estimate energy barriers from the reaction energy alone. However, to carry out a systematic screening of other metallic (and bimetallic) surfaces still involves a significant computational effort. In order to further reduce this task, we plot E_{act} versus the co-adsorption energy of H^* and OH^* (Fig. 3b). The new relationship provides a simpler descriptor since E_{act} can be estimated from the reaction products E_{ads} without requiring the corresponding value for the reactant. Inspired by the work of Nørskov et al. on C_2H_2 to C_2H_4 selective hydrogenation [47] and on scaling relationships [48], we have also investigated the relationship between E_{act} for the surface-catalyzed water splitting reaction and the adsorption energy of atomic O. The plot in Fig. 3c shows that adsorption energy of a species that is not involved in the reaction provides a simple and convenient descriptor allowing to estimate the energy barriers in a direct way.

The validity of the present relationships was confirmed by comparing E_{act} values estimated from equations in Fig. 3 to the explicit calculation of energy barriers for the $H_2O^* + * \rightarrow HO^* + H^*$ reaction on some additional TM surfaces not included in the original fitting. These correspond to the Ru(0 0 0 1), Rh(2 2 1) and Pd(1 1 0) surfaces whereas three additional cases – Ir(1 1 0), Co(0 0 0 1) and Co(1 1 1) – are estimated from the BEP relationships (see Table 2 for numerical results and Fig. 4 for optimized configurations of co-adsorbed $HO^* + H^*$ on Ru(0 0 0 1), Rh(2 2 1), Ir(1 1 0), Co(0 0 0 1) and Co(1 1 1) surfaces). Thus, the eleven topmost rows of Table 2 show that the E_{act} values estimated from the relationships in Fig. 3 differ from the explicitly calculated values by at most 0.19 eV with mean deviations (Δ) of 0.08–0.12 eV depending on the relationship used for data estimation. Note that these Δ values are close to (or even larger than) those obtained with the multilinear least square regression. This indicates that other regression methods could lead to Δ values lower than those arising from a simple linear regression. Nevertheless, the goal of the present paper is no to propose different types of eventually more accurate relationships but to show that physically meaningful BEP relationships hold, at least in a semi-quantitative way, and that the adsorption energy of atomic oxygen provides an appropriate descriptor for the activity of metal surfaces toward water dissociation.

Table 2
Calculated (TS calculation) and estimated (equations in Fig. 3) energy barriers for the water dissociation on several surfaces. Values in eV and differences to the TS calculated values in parenthesis.

Surface	TS	BEP (E_{react})	$E_{ads}(OH^* + H^*)$	$E_{ads}(O^*)$
Ir(1 1 1)	0.68	0.85 (0.17)	0.85 (0.17)	0.74 (0.06)
Ni(1 1 1)	0.71	0.62 (−0.09)	0.66 (−0.05)	0.55 (−0.16)
Pd(1 1 1)	0.96	0.84 (−0.12)	0.85 (−0.11)	0.85 (−0.11)
Pt(1 1 1)	0.78	0.91 (0.13)	0.92 (0.14)	0.89 (0.10)
Cu(1 1 1)	0.91	0.77 (−0.15)	0.80 (−0.11)	0.78 (−0.14)
Ni(1 1 0)	0.39	0.57 (0.18)	0.56 (0.18)	0.58 (0.19)
Cu(1 1 0)	0.61	0.73 (0.12)	0.73 (0.12)	0.58 (0.03)
Ag(1 1 0)	1.12	0.96 (−0.16)	0.95 (−0.17)	1.09 (−0.03)
Rh(2 1 1)	0.67	0.60 (−0.07)	0.59 (−0.09)	0.63 (−0.04)
Ni(2 1 1)	0.61	0.52 (−0.09)	0.50 (−0.11)	0.60 (−0.01)
Cu(3 2 1)	0.71	0.79 (0.08)	0.74 (0.03)	0.70 (−0.01)
Pd(1 1 0)	0.73[a]		0.75[b]	0.89[b]
Rh(2 2 1)	0.65[a,c]		0.60[b]	0.68[b]
Ru(0 0 0 1)	0.80[a,d,e]; 0.85[a,d,f]; 0.90[a,d,g]		0.64[b]; 0.84[d]	0.55[b]; 0.77[d]
Ir(1 1 0)			0.56[b]	0.73[b]
Co(0 0 0 1)			0.63[b]	0.50[b]
Co(1 1 1)			0.63[b]	0.49[b]

[a] Explicitly calculated but not included in the fit.
[b] Estimated value.
[c] DFT-PW91 value from Ref. [21];
[d] Value without ZPVE corrections;
[e] DFT-PW91 values from Ref. [51] on 2 × 2 cells.
[f] DFT-PW91 values from Ref. [51] on 3 × 3 cells.
[g] DFT-PBE value from Ref. [19].

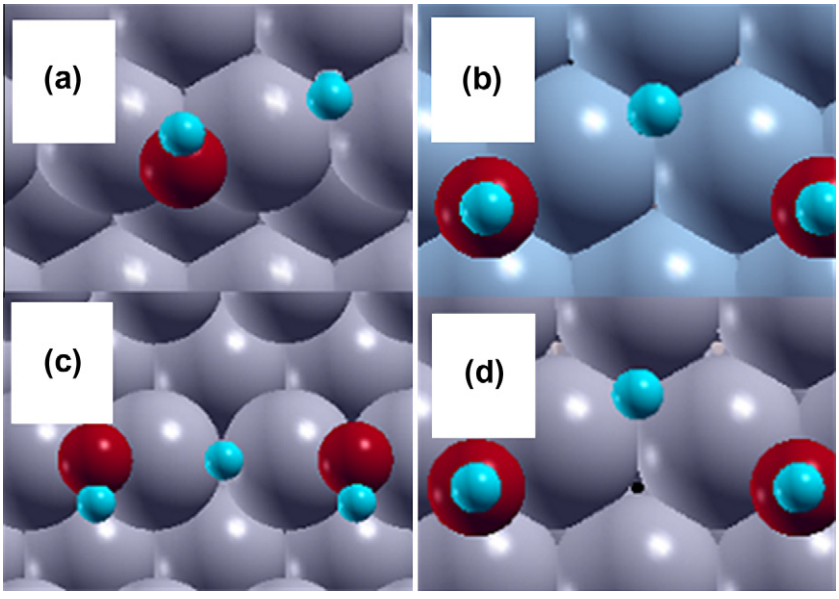

Fig. 4. Most stable configurations for the OH + H pair co-adsorption on the (a) Rh(2 2 1), (b) Co(1 1 1), (c) Ir(1 1 0) and (d) Ru(0 0 0 1) surfaces. The most stable configuration for the OH + H co-adsorption on the Co(0 0 0 1) surface is close to that in (b) and it was omitted.

It is also rather encouraging to see that values determined with the present relationships for Ru(0 0 0 1), Rh(2 2 1) surfaces are in good agreement with energy barriers calculated by other authors [19,21,51] from the corresponding calculated energy profile and TS structures and that the predicted values for Pd(1 1 0) are consistent with the explicitly calculated values in this work but not used in the fit. Furthermore, from estimated data in Table 2, it is possible to conclude that cobalt may be also an interesting material for the WGS without direct dependency on the nature of the support like it happens with gold-based catalysts. Since calculated (co-)adsorption energies of $OH^* + H^*$ and O^* species on the two Co surfaces are identical, the estimated energy barriers are also the same and these two allomorphic forms are expected to have similar activity during WGS low and high temperature cycles.

Additional useful relationships are also found between the calculated rate constants and the E_{ads} of selected species or between the rate constants and E_{react} (Fig. 5). These new types of relationships allow for a direct estimation of the water splitting reaction rate constant on a given surface from the adsorption energy of atomic oxygen only. In fact, using the relationship in Fig. 5b (or relationships in Figs. 5a or 5c) allows us to estimate the rate constants for water dissociation on Rh(2 2 1), Co(0 0 0 1), Co(1 1 1), Pd(1 1 0), Ir(1 1 0) and Ru(0 0 0 1) surfaces, which are $8.0 \times 10^5\ s^{-1}$ ($1.0 \times 10^5\ s^{-1}$), $4.0 \times 10^5\ s^{-1}$ ($7.0 \times 10^6\ s^{-1}$), $4.1 \times 10^5\ s^{-1}$ ($7.6 \times 10^6\ s^{-1}$), $2.2 \times 10^4\ s^{-1}$ ($9.3 \times 10^2\ s^{-1}$), $1.9 \times 10^6\ s^{-1}$ ($3.3 \times 10^4\ s^{-1}$) and $2.8 \times 10^5\ s^{-1}$ ($2.0 \times 10^6\ s^{-1}$), respectively.

A final comment is necessary to rationalize the existence and usefulness of the present BEP relationships. A first comment concerns whether these can be anticipated from arguments arising from the d-band model [44,45]. However, one must advert that this otherwise extremely useful concept has to be used with extreme care. In fact, the d-band model allows one to understand the trends in adsorption of a given adsorbate on different surfaces of the same element but does not normally hold when comparing different elements [49]. This is also the case for the surfaces explored in the present work. Fig. 6 shows that the correlation between E_{act} and the center of the d-band is extremely poor when including all calculated data. On the contrary, a fairly good correlation is found when considering Cu(1 1 1), Cu(1 1 0) and Cu(3 2 1) or Ni(1 1 1), Ni(1 1 0) and Ni(2 1 1). This analysis clearly shows that the d-band model cannot be used to understand the origin of the BEP relationship described above. In principle, they seem to follow the general rule that, taking the adsorbed reactants as origin, stabilizing the products tends to lower the energy barrier for the reaction. This holds for the BEP using OH^* and H^* and it is not surprising that this is also related to the BEP using O^* because adsorption of atomic oxygen and of hydroxyl involve a similar chemistry. However, one must be aware that there are also exceptions to this general behavior [22,50]. In a similar way, one must be aware that the existence of the BEP relationships described above provides just a starting point toward the design of new catalysts which must be followed by a complete study of the full reaction mechanism and

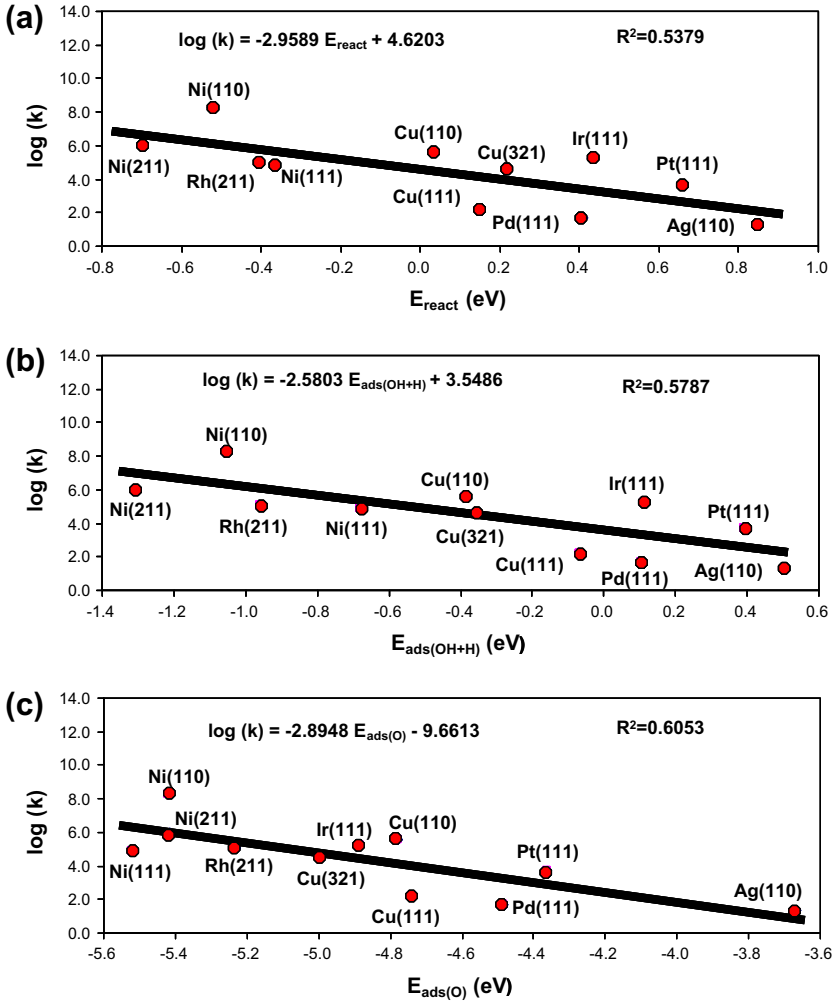

Fig. 5. Relationships between the logarithm of the rate constant (log k) and (a) E_{react} of the $H_2O^* + * \rightarrow OH^* + H^*$ reaction. (b) Co-adsorption energy of HO and H species; (c) E_{ads} of atomic oxygen.

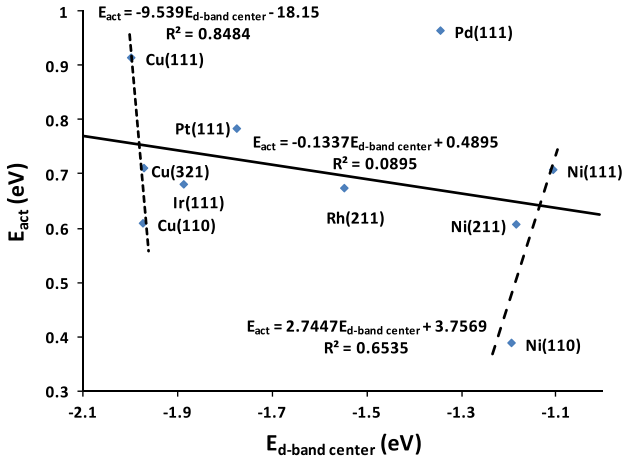

Fig. 6. Full line shows a plot of the calculated activation energy (E_{act}) for water dissociation catalyzed by various metal surfaces versus the energy of the center of the d-band ($E_{d\text{-band center}}$). Note that meaningful correlations (dashed lines) do only show up when considering different surfaces of the same element (e.g. copper or nickel). Values for Au and Ag surfaces are not included.

pertinent microkinetic analysis of the performance of selected candidates under realistic working conditions.

4. Conclusions

Periodic density functional calculations have been used to explore the catalytic activity of various metallic surfaces toward water dissociation. The surfaces investigated include the most stable ones but also a wide range of stepped and folded surfaces thus allowing us to explicitly take into account the effect of low coordinated sites on the energy profile. These calculations allowed us to extract a series of general conclusions. First, among the different surfaces considered in this work, Au is confirmed as the least active for water dissociation while Co and Ni seem to be interesting and cheap candidates for the WGS (or simply to split water) although one has to keep in mind that these metals are usually employed in hydrogenation reactions and, hence, selectivity needs to be further considered. Second, the presence of low coordinated atoms increases the adsorption energies of water and of the reaction products with a concomitant reduction of the activation energies for the water dissociation. Third, the activation energy for water dissociation at these metallic surfaces follows a BEP relationship. The validity of the BEP relationships have been confirmed by explicit calculation of a few additional cases not included initially in the derivation of such relationship. Fourth, the adsorption energy of atomic oxygen on a given metallic surface provides an excellent descriptor of the activation energy thus allowing the screening of a large number of metallic (and bimetallic) systems in a simple way. These relationships are likely to provide one more useful step in the complex process of finding new catalysts for the WGS and related processes.

Acknowledgments

We acknowledge FEDER, FSE, FCT, CRUP and MICCIN for a postdoctoral Grant (SFRH/BPD/27167/2006) and Projects E-43/08, FIS2008-02238 and HP2007-0042.

Appendix A. Supplementary material

Data concerning the adsorption of H_2O, OH+H and O and also the TS appear in Tables S1-S4, respectively, while Table 5 presents the vibrational modes for reactants, TS and products of the reaction of water dissociation. Tables S6 and S7 present the statistical analyses for the equations in the text. Table S8 compiles the available experimental adsorption energies for atomic oxygen. Figures S1 and S2 show the correlations between calculated and experimental adsorption energies of O on (1 1 1) surfaces and between the activation energy barrier and the calculated or experimental adsorption energies of atomic oxygen. Finally, it is presented the approach used for the calculation of the Gibbs energies. Supplementary data associated with this article can be found, in the online version, at doi:10.1016/j.jcat.2010.09.007.

References

[1] A.Y. Rozovskii, G.I. Lin, Top. Catal. 22 (2003) 137.
[2] M.A. Larrubia-Vargas, G. Busca, U. Costantino, F. Marmottini, T. Montanari, P. Patrono, F. Pinzari, G. Ramis, J. Mol. Catal. A: Chem. 266 (2007) 188.
[3] S.H.D. Lee, D.V. Applegate, S. Ahmed, S.G. Calderone, T.L. Harvey, Int. J. Hydrogen Energy 30 (2005) 829.
[4] D.J. Suh, C. Kwak, J.-H. Kim, S.M. Kwon, T.-J. Park, J. Power Sour. 142 (2005) 70.
[5] C.V. Ovesen, B.S. Clausen, B.S. Hammershøi, G. Steffensen, T. Askgaard, I. Chorkendorff, J.K. Nørskov, P.B. Rasmussen, P. Stoltze, P.J. Taylor, J. Catal. 158 (1996) 170.
[6] N. Schumacher, A. Boisen, S. Dahl, A.A. Gokhale, S. Kandoi, L.C. Grabow, J.A. Dumesic, M. Mavrikakis, I. Chorkendorff, J. Catal. 229 (2005) 265.
[7] Q. Fu, H. Saltsburg, M. Flytzani-Stephanopoulos, Science 301 (2003) 935.
[8] J.A. Rodríguez, J. Evans, J. Graciani, J.-B. Park, P. Liu, J. Hrbek, J. Fdez Sanz, J. Phys. Chem. C 113 (2009) 7364.
[9] L. Li, Y. Zhan, Q. Zheng, Y. Zheng, X. Lin, D. Li, J. Zhu, Catal. Lett. 118 (2007) 91.
[10] H. Yahiro, K. Murawaki, K. Saiki, T. Yamamoto, H. Yamaura, Catal. Today 126 (2007) 436.
[11] J.A. Rodriguez, P. Liu, X. Wang, W. Wen, J. Hanson, J. Hrbek, M. Pérez, J. Evans, Catal. Today 143 (2009) 45.
[12] X. Wang, J.A. Rodriguez, J.C. Hanson, D. Gamarra, A. Martínez-Arias, M. Fernández-García, J. Phys. Chem. B 110 (2006) 428.
[13] J.A. Rodriguez, S. Ma, P. Liu, J. Hrbek, J. Evans, M. Pérez, Science 318 (2007) 1757.
[14] J.B. Park, J. Graciani, J. Evans, D. Stacchiola, S.D. Senanayake, L. Barrio, P. Liu, J.F. Sanz, J. Hrbek, J.A. Rodriguez, J. Am. Chem. Soc. 132 (2010) 356.
[15] A. Gokhale, J.A. Dumesic, M. Mavrikakis, J. Am. Chem. Soc. 130 (2008) 1402.
[16] J.L.C. Fajín, M.N.D.S. Cordeiro, F. Illas, J.R.B. Gomes, J. Catal. 268 (2009) 131.
[17] J.N. Brønsted, Chem. Rev. 5 (1928) 231.
[18] M.G. Evans, M. Polanyi, Trans. Faraday Soc. 34 (1938) 11.
[19] J.G.-C. Wang, S.-X. Tao, X.-H. Bu, J. Catal. 244 (2006) 10.
[20] A.A. Phatak, W.N. Delgass, F.H. Ribeiro, W.F. Schneider, J. Phys. Chem. C 113 (2009) 7269.
[21] P.W. van Grootel, E.J.M. Hensen, R.A. van Santen, Surf. Sci. 603 (2009) 3275.
[22] V. Pallassana, M. Neurock, J. Catal. 191 (2000) 301.
[23] J.K. Nørskov, T. Bligaard, A. Logadottir, S. Bahn, L.B. Hansen, M. Bollinger, H. Bengaard, B. Hammer, Z. Sljivancanin, M. Mavrikakis, Y. Xu, S. Dahl, C.J.H. Jacobsen, J. Catal. 209 (2002) 275.
[24] D. Loffreda, F. Delbecq, F. Vigné, P. Sautet, Angew. Chem. Int. Ed. 48 (2009) 8978.
[25] R.A. van Santen, M. Neurock, S.G. Shetty, Chem. Rev. 110 (2010) 2005.
[26] B.L.M. Hendriksen, M.D. Ackermann, R. van Rijn, D. Stoltz, I. Popa, O. Balmes, A. Resta, D. Wermeille, R. Felici, S. Ferrer, J.W.M. Frenken, Nature Chem. 2 (2010) 730.
[27] V.R. Saunders, R. Dovesi, C. Roetti, M. Causà, N.M. Harrison, R. Orlando, C.M. Zicovich-Wilson, Computer Code CRYSTAL 98, User's Manual (University of Torino), Torino, 1998.
[28] G. Kresse, J. Hafner, Phys. Rev. B 47 (1993) 558.
[29] G. Kresse, J. Furthmüller, Comput. Mater. Sci. 6 (1996) 15.
[30] G. Kresse, J. Furthmüller, Phys. Rev. B 54 (1996) 11169.
[31] J.P. Perdew, J.A. Chevary, S.H. Vosko, K.A. Jackson, M.R. Pederson, D.J. Singh, C. Fiolhais, Phys. Rev. B 46 (1992) 6671.
[32] P.E. Blöchl, Phys. Rev. B 50 (1994) 17953.
[33] G. Kresse, D. Joubert, Phys. Rev. B 59 (1999) 1758.
[34] H.J. Monkhorst, J.D. Pack, Phys. Rev. B 13 (1976) 5188.
[35] O. Diéguez, N. Marzari, Phys. Rev. B 80 (2009) 214115.
[36] S. Meng, E.G. Wang, S. Gao, Phys. Rev. B 69 (2004) 195404.
[37] J.L.C. Fajín, F. Illas, J.R.B. Gomes, J. Chem. Phys. 130 (2009) 224702.
[38] J.L.C. Fajin, M.N.D.S. Cordeiro, J.R.B. Gomes, J. Phys. Chem. C 111 (2007) 17311.
[39] V.A. de la Peña O'Shea, S. González, F. Illas, J.L.G. Fierro, Chem. Phys. Lett. 454 (2008) 262.
[40] C. Kittel, in: Introduction to Solid State Physics, seventh ed., Wiley, New York, 1996, p. 449.
[41] G. Rahman, I.G. Kim, J. Magn. 13 (2008) 124.
[42] G. Henkelman, H. Jónsson, J. Chem. Phys. 111 (1999) 7010.
[43] K.J. Laidler, in: Chemical Kinetics, third ed., Harper Collins, New York, 1987, p. 193.

[44] B. Hammer, J.K. Nørskov, Surf. Sci. 343 (1995) 211.
[45] B. Hammer, J.K. Nørskov, Surf. Sci. 359 (1996) 306.
[46] E.D. German, M. Sheintuch, J. Phys. Chem. C 114 (2010) 3089.
[47] F. Studt, F. Abild-Pedersen, T. Bligaard, R.Z. Sørensen, C.H. Christensen, J.K. Nørskov, Science 320 (2008) 1320.
[48] F. Abild-Pedersen, J. Greeley, F. Studt, J. Rossmeisl, T.R. Munter, P.G. Moses, E. Skulason, T. Bligaard, J.K. Nørskov, Phys. Rev. Lett. 99 (2007) 1016105.
[49] M. Mavrikakis, B. Hammer, J.K. Norskov, Phys. Rev. Lett. 81 (1998) 2819.
[50] J.R.B. Gomes, J.M. Bofill, F. Illas, J. Phys. Chem. C 112 (2008) 1072.
[51] A. Michaelides, A. Alavi, D.A. King, J. Am. Chem. Soc. 125 (2003) 2746.